Surface Science 604 (2010) 718–729

Contents lists available at ScienceDirect

Surface Science

journal homepage: www.elsevier.com/locate/susc

Hydrogen adsorption on palladium and palladium hydride at 1 bar

M. Johansson [a], E. Skúlason [b], G. Nielsen [a], S. Murphy [a], R.M. Nielsen [a], I. Chorkendorff [a,*]

[a] Danish National Research Foundation's Center for Individual Nanoparticle Functionality (CINF), Dept. of Physics, Nano-DTU, Technical University of Denmark (DTU), Building 312, Kgs. Lyngby 2800, Denmark
[b] Center for Atomic-scale Materials Design (CAMD), Dept. of Physics, Nano-DTU, Technical University of Denmark (DTU), Building 311, Kgs. Lyngby 2800, Denmark

ARTICLE INFO

Article history:
Received 2 September 2009
Accepted for publication 22 January 2010
Available online 2 February 2010

Keywords:
DFT
Adsorption
Palladium
Hydrogen
Polycrystalline

ABSTRACT

The dissociative sticking probability for H_2 on Pd films supported on sputtered Highly Ordered Pyrolytic Graphite (HOPG) has been derived from measurements of the rate of the H–D exchange reaction at 1 bar. The sticking probability for H_2, S, is higher on Pd hydride than on Pd (a factor of 1.4 at 140 °C), but the apparent desorption energy derived from S is the same on Pd and Pd hydride within the uncertainty of the experiment. Density Functional Theory (DFT) calculations for the (1 1 1) surfaces of Pd and Pd hydride show that, at a surface H coverage of a full mono layer, H binds less strongly to Pd hydride than to Pd. The activation barrier for desorption at a H coverage of one mono layer is slightly lower on Pd hydride, whereas the activation energy for adsorption is similar on Pd and Pd hydride. It is concluded that the higher sticking probability on Pd hydride is most likely caused by a slightly lower equilibrium coverage of H, which is a consequence of the lower heat of adsorption for H on Pd hydride.

1. Introduction

Palladium is used industrially as a catalyst for, e.g. hydrogenation reactions and exhaust gas cleaning, and is unique among the metals because it combines a high activity for hydrogen splitting with a high solubility for hydrogen in the bulk. An interesting question is to what extent the presence of H in the bulk of Pd will change parameters such as the heat of adsorption and the equilibrium coverage of H on the surface, and ultimately how it will influence the reactivity of a real catalyst. The issue has been the subject of a number of recent publications [1–7]. This contribution addresses the question of how the formation of Pd hydride in the metal bulk affects the dissociation rate of H_2 on the Pd surface.

There exist a large number of studies of hydrogen adsorption on Pd surfaces under ultra-high vacuum (UHV) conditions [8–19]. Values for the heat of adsorption at low H coverage between 90 and 127 kJ/mole H_2 have been reported [8,14,18,19]. In general, the heat of adsorption is found to decrease with increasing hydrogen surface coverage [8,13,14,18]. Usually, the heat of adsorption is given as a function of work function shift rather than coverage. The only study where the H surface coverage is quantified is made on Pd(1 0 0), where the heat of adsorption drops to 70.4 kJ/mole H_2 at a H coverage corresponding to 1.3 mono layer (ML) [14].

The absorption of hydrogen in Pd has been investigated extensively, see for example [20–25]. It is found that below a critical temperature of 298 °C, there exist two phases, a solid solution of H in Pd, the α-phase, and the Pd hydride or β-phase. These two phases coexist over a broad concentration range [20,22]. The heat of absorption in the limit of zero bulk H concentration is 19 kJ/mole H_2 [21] and is thus significantly lower than the heat of adsorption on the surface. This means that the adsorption sites on the surface will fill before those in the bulk as the hydrogen pressure is increased. The lattice constant for Pd increases by about 3.5% on formation of the β-phase, which causes tensile strain to the lattice [26,27].

The measurements of the heat of adsorption cited above were made at pressures below 1×10^{-5} Torr and temperatures above room temperature. From extrapolation in the phase diagram for the H/Pd system the corresponding equilibrium atomic concentration of H in the bulk is below 1% [20]. Below the critical temperature of 300 °C this is in the α-phase region of the phase diagram [20,21]. Due to the slow diffusion of H in Pd at temperatures below room temperature, it is difficult to obtain equilibrium between surface and bulk at the temperatures necessary to create the β-phase under vacuum conditions. However, hydrogen absorbed in the bulk close to the surface, frequently referred to as 'surface hydride', has been observed in TPD studies where hydrogen is dosed below room temperature [9,11,12,19]. The only study of hydrogen adsorption on β-phase Pd hydride which we are aware of was made on a polycrystalline foil which was loaded at 2000 Torr hydrogen pressure, cooled, and transferred to a UHV chamber [28]. The activation energy for desorption was determined to be 33.8 kJ/mole H_2 for a constant, but not specified, hydrogen surface coverage [28].

* Corresponding author. Tel.: +45 45253170.
E-mail address: ibchork@fysik.dtu.dk (I. Chorkendorff).

0039-6028/$ - see front matter © 2010 Elsevier B.V. All rights reserved.
doi:10.1016/j.susc.2010.01.023

There are a number of DFT studies of the electronic properties of Pd surfaces in the presence of hydrogen, quantified by electron densities or the local density of states of the surface atoms [29–36]. The adsorption energy has been calculated for various H coverages and surfaces [29–35,37–41]. Values for the adsorption energy at low coverage fall in the range of 83–138 kJ/mole H_2 [30,31,34,37–41], with only a small decrease with H coverage up to 1 ML [30,37,38,40]. With the exception of Ref. [34] all the published studies agree with experiments in that the fcc-hollow site is the most favorable adsorption site on the Pd(1 1 1)-surface for H coverages below 1 ML, [30,32,33,35,37–39,41–43]. Palladium hydride has also been computationally characterized [44,45], but to a much lesser extent than Pd.

The kinetics of adsorption have been investigated with molecular beam techniques and it was found that both activated and unactivated adsorption paths are present on the clean surfaces of Pd(1 1 1), Pd(1 1 0) and Pd(1 0 0) [16,17]. This is in agreement with theoretical studies where both activated and non-activated pathways were found by calculating the full potential energy surface with DFT [33]. More recent studies have investigated H_2 dissociation at high hydrogen surface coverage, originated by a STM study by Mitsui et al. [43,46], where it was found that at high coverage, adsorption does not occur on vacancy dimers. Instead, an ensemble of more than two vacancies is necessary [43,46]. Density Functional Theory (DFT) calculations indicate that an ensemble of three vacancies, where a Pd atom does not bind directly to H gives a lower barrier for desorption than a vacancy dimer [40]. Molecular dynamics calculations of H_2 adsorption on Pd(1 1 1) and Pd(1 0 0) confirm that adsorption on the H covered surfaces does not occur on vacancy dimers under the conditions studied by Mitsui et al. However, adsorption will occur on vacancy dimers for kinetic energies above 0.1 eV, even though the trimer is still more active [47].

Here we report an experimental study of the sticking probability and the apparent desorption energy for H_2 on Pd and Pd hydride at a hydrogen pressure of 1 bar in the temperature interval 25–200 °C. The experiments are carried out on polycrystalline Pd films supported on a sputtered Highly Ordered Pyrolytic Graphite (HOPG) substrate. The main motive for choosing HOPG as a substrate is that graphite is used as substrate in Proton Exchange Membrane (PEM) fuel cells. In order to account for the effects seen experimentally, DFT calculations of the adsorption energies and the activation barriers for adsorption and desorption of hydrogen on the (1 1 1) and (2 1 1) facets of Pd and on the (1 1 1) facet of Pd hydride are carried out. The objective has not been to perform a full investigation of the two systems, but to make a comparative analysis of the energies upon desorption and adsorption of H_2 on the (1 1 1) surfaces, and to use the (2 1 1) surface to investigate the influence of steps.

The experiments show that the sticking probability is higher for Pd hydride than for Pd. However, within the experimental uncertainty, the apparent desorption energy is the same for Pd and Pd hydride. The DFT calculations indicate that H binds weaker to Pd hydride than to Pd and that the activation energy for desorption is slightly lower on Pd hydride. It is concluded that the reason for the higher sticking probability on Pd hydride as compared to Pd is a slightly lower hydrogen coverage on Pd hydride, caused by the lower heat of adsorption for H on Pd hydride.

2. Experimental details

The apparatus used in this investigation consists of an ultra-high vacuum chamber equipped with a high pressure cell and has been described in detail in a previous publication [48]. In the vacuum chamber, model catalysts in the form of circular metal films are manufactured by electron beam evaporation of metals onto a substrate. The vacuum chamber is also used for characterization of the metal films with Auger Electron Spectroscopy (AES) and Scanning Electron Microscopy (SEM). In the high pressure cell, the individual catalytic activity of the metal films is tested by measuring the local gas composition over the catalytic surface. Fig. 1 shows the principles of the high pressure experiment. The gas is sampled with a quartz capillary leak, made from a 1 mm o.d. quartz tube, and analyzed with mass spectrometry. The quartz tube is mounted concentrically in the gas inlet nozzle, see Fig. 1, and gas is blown toward the sample surface through the annulus between the capillary and the nozzle. The entire gas sampling device can be moved in three dimensions over the sample. When the sampling device is positioned over the center of one of the metal films, the gas flow will prevent products formed on the other films from influencing the measurement [49]. The substrate is a 7 mm by 7 mm Highly Ordered Pyrolytic Graphite (HOPG) sample which is glued (Graphi-Bond 669, Aremco Products) onto a graphite disc, 10 mm in diameter and about 2 mm thick. The graphite disc is mounted on two tungsten filaments, which are used for heating. The sample temperature is measured with a thermocouple glued onto the graphite disc at the edge of the HOPG sample, see Fig. 1. The gases used are N60 (99.9999%) H_2 and 99.8% D_2 (main contaminant HD) which are additionally purified by guard catalysts [50]. In order to avoid contamination by sulfur, the high pressure cell was cleaned by flowing hydrogen through it at 1 bar for 48 h during bake-out at 150 °C.

The experimental procedures have been described in detail in a previous publication [50]. In short, the HOPG sample is cleaned by Ar sputtering for several hours between experiments, followed by heating to 800 °C for 20 min to desorb any remaining Ar from the

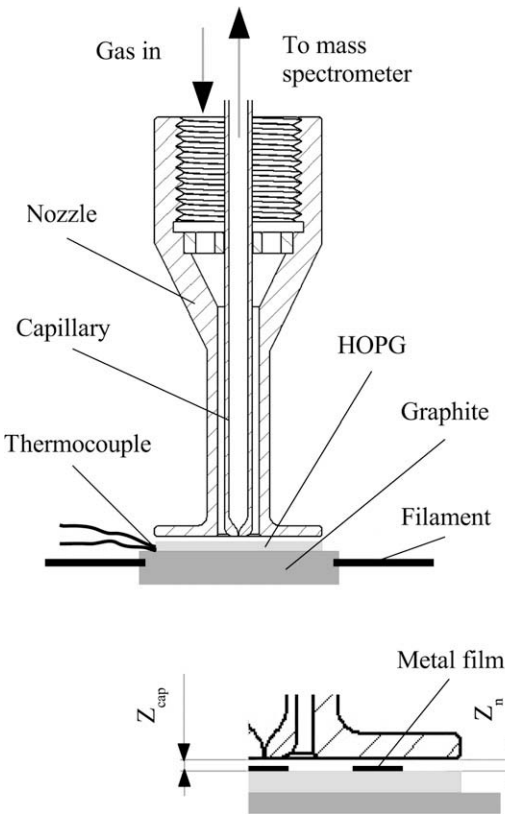

Fig. 1. The gas sampling device positioned over a sample with metal films. The thickness of the films has been exaggerated in the figure. The distance between the tip of the capillary, where the leak is situated, and the sample surface, Z_{cap}, is 0.2 mm, as is the distance between the nozzle and the sample surface, Z_n.

sample. The metal films are evaporated with the substrate at room temperature and an evaporation rate of 5–10 Å/min. The thickness of the films is 50 Å and the diameter 1 mm. After evaporation, the sample is kept at 150 °C, in order to avoid adsorption of background gas. The cleanliness of the films is checked with AES before the sample is moved to the high pressure cell [50].

Fig. 2 shows STM images of a 50 Å thick Pd film. The film was exposed to 1 bar of H_2 in the high pressure cell for 1 h prior to transfer to the STM in air. The ridge-like structure is a feature of the substrate and is caused by the sputtering. The Pd film is probably not continuous, since C is always present in the Auger spectra. However, it is difficult to quantify the amount of carbon, due to the peak overlap between C and Pd. In a similar study including the metals Ir, Pt, Co and Ni, which do not give peak overlap, it was concluded that C is present in the Auger spectra at atomic concentrations between 4% and 25% [50].

The high pressure measurements are carried out with a mixture of 1% D_2 in H_2 at 1 bar total pressure. The sample was first kept in the high pressure cell at 1 bar and 200 °C for at least 1 h, which is the time needed to align the gas sampling device. The measurements were then carried out for decreasing temperatures starting at 200 °C. To safeguard against changes in the reaction rate due to, e.g., contamination or structural changes of the surfaces, the first measurement was repeated at the end of the series. The total exposure time in the high pressure cell varied between 4 and 24 h.

After the high pressure experiment, the sample was transferred back to the main chamber for AES analysis, while kept at 150 °C. No contaminants other than C were detected after the high pressure experiment. From the AES spectra, it seems that the amount of C often increases somewhat during the high pressure experiment. This could indicate restructuring of the films or migration of carbon from the support onto the metal surface.

The mass spectrometer signals for H_2 and D_2 were calibrated using the signals measured over the graphite substrate, where the gas composition is the same as in the gas fed to the high pressure cell [49]. For HD, the calibration factor was obtained by comparing calculated HD pressures to the measured, background corrected HD signal [51]. The uncertainty in the partial pressures of H_2 and D_2, p_{H_2} and p_{D_2}, is about 1% [51]. The dominating source of error when determining the calibration factor for HD is the uncertainty in the position of the capillary and the nozzle relative to the sample surface. This gives an uncertainty in the absolute value for the HD pressure, p_{HD}, of ±10% [51].

A simple model is used in order to describe the net HD production rate as a function of the partial pressures at the catalytic surface [51]. It is assumed that the sticking probability, S, has the same value irrespective of whether the adsorbing molecule is H_2, HD or D_2, and that it does not depend on the H/D ratio on the surface. Since the experiments are made with only 1% D_2, the total hydrogen coverage is assumed to equal that corresponding to 1 bar of pure H_2.

It is furthermore assumed that the desorption rates r_{HH}, r_{HD} and r_{DD} fulfill

$$r_{HD} = \sqrt{K_F r_{HH} r_{DD}} \tag{1}$$

where the flux equilibrium constant, K_F, is given by

$$K_F = K_g \frac{\sqrt{m_{H_2} m_{D_2}}}{m_{HD}} \tag{2}$$

and K_g is the equilibrium constant for the gas phase reaction

$$H_2 + D_2 \rightleftharpoons 2HD \tag{3}$$

[51].

Eq. (1) is, for example, fulfilled if the desorption rates are proportional to the products of the coverages of H and D, θ_H and θ_D,

$$r_{ij} = k_{ij}\theta_i\theta_j; \quad i, j = H, D \tag{4}$$

and the k_{ij} are rate constants derived from transition state theory (TST) [51].

In principle, S might differ between the different species due to, e.g., different differences between the entropy for the transition state and that of the gas phase. Differences in the sticking probability for H_2, HD and D_2 can be taken into account in the model [51]. However, we have not been able to find any useful experimental data in the literature. The presence of an activation barrier for adsorption could also give rise to differences in the sticking probability for H_2, HD and D_2 [52]. Whether the sticking probabilities will be different or not depends on the ground state energy of the transition state for adsorption of H_2, HD and D_2 relative to the ground state of the molecules in the gas phase. Since it is presently not clear whether there is an activation barrier for adsorption on the surfaces studied, see Section 4.2.2, no attempt was made to include such effects in the data evaluation.

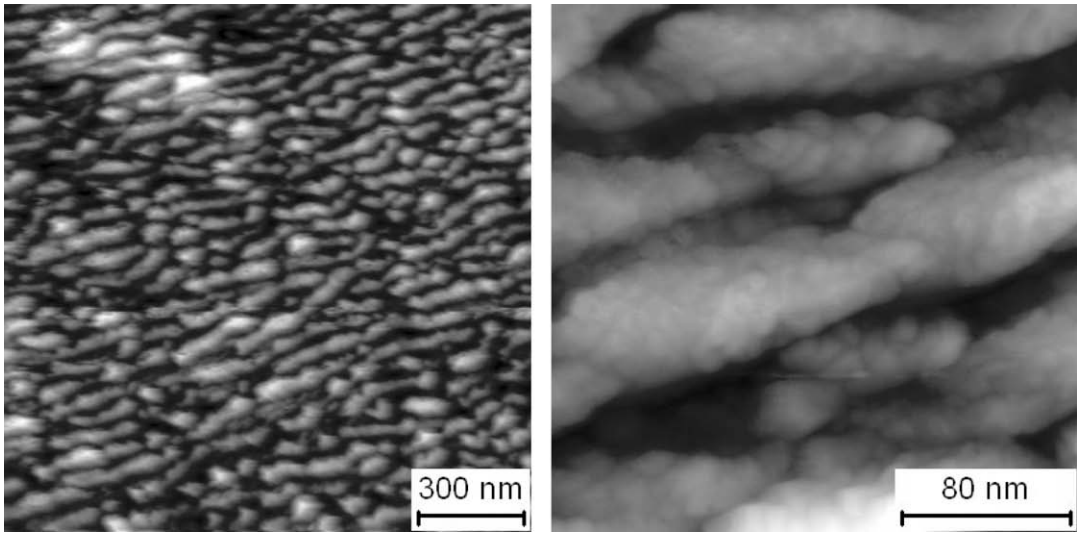

Fig. 2. STM images of a 50 Å thick Pd film. The images were obtained by an Omicron UHV STM after transfer in air. The tunnel currents were 600 and 800 pA for the left and right image, respectively. The corresponding bias voltages were 0.1 and 1.8 V, respectively.

The model for the HD production rate at the Pd surface is used in computational fluid dynamics simulations which yield the gas composition distribution in the volume over the sample. The result of interest is the gas composition at the point of measurement (the tip of the capillary) as a function of S [49,51]. With knowledge of this relation, S can be obtained from measured gas compositions by interpolation. The partial pressure of D_2, p_{D_2}, was used to calculate S, if the lowering in p_{D_2} relative to the D_2 pressure over the graphite surface (the partial pressure in the gas fed to the high pressure cell) was more than 8%, otherwise the HD pressure was used to determine S. In the latter case, the calibration factor for the HD signal was obtained from a measurement where p_{D_2} could be used to obtain S.

The lower detection limit for the HD pressure is determined by the sensitivity limit of the mass spectrometer, which is only about 0.1 mbar in this case, due to the background of H_3^+ formed in the ion source. The detection limit corresponds to $S \approx 5 \times 10^{-6}$ [51].

3. Experimental results

Fig. 3 shows the HD signal (3 AMU) obtained in an experiment with one Pt and one Pd film. The results for Pt are not relevant to this study, but were published elsewhere [51]. At $t = 0$ min, the gas sampling device is positioned 0.2 mm over the center of the Pd film. The temperature is 200 °C and the total pressure 1 bar. The insert shows the HD signal during one measurement cycle: The gas sampling device is moved from the center of the Pd film to the center of the Pt film and then to a point over the graphite sample, well away from the metal films, to obtain a measurement of the background level. Finally, the gas sampling device is moved back to the Pd film and the temperature is changed before the cycle is repeated. Thus, apart from the time spent over Pt and C, the HD signal reflects the activity of the Pd film.

As can be noted from Fig. 3, the approach to steady state is slow after lowering/raising the temperature to 140 °C. The time to achieve steady state after a change in temperature varied in a seemingly random way between experiments. In some cases it was observed to be more than 10 min. Typically, the approach to steady state was slow close to the temperature range where the α- and β-phases coexist, see Section 3.1. It is known that the time needed for the formation/destruction of the β-phase depends sensitively on the surface conditions, and can be many hours, or even days, at room temperature for bulk samples [53]. For the experiment shown in Fig. 3 it is believed that steady state was achieved after changes in the temperature, except for the points at 140 and 160 °C, since the values for increasing and decreasing temperature agree, within the uncertainty of the experiment. The difference between the values for increasing and decreasing temperature at 140 and 160 °C could either be due to a too short measurement time or to hysteresis.

Fig. 4 shows the partial pressure of HD, p_{HD}, over the center of a Pd film as a function of the temperature, T. The measurements were carried out first for decreasing and then for increasing temperatures. In this measurement the cycle time was as short as possible, or about 200 s. As is clear from Fig. 4, the time to achieve steady state was shorter in this experiment, since the data for increasing and decreasing temperature agree, with the exception of the value for 140 °C at 1 bar. As a matter of fact, there appears to be an interval of hysteresis around 140 °C at 1 bar. In order to check whether the interval of hysteresis moved to lower temperatures with decreasing pressure, experiments were also performed at 0.5 and 0.1 bar. The data is shown in Fig. 4.

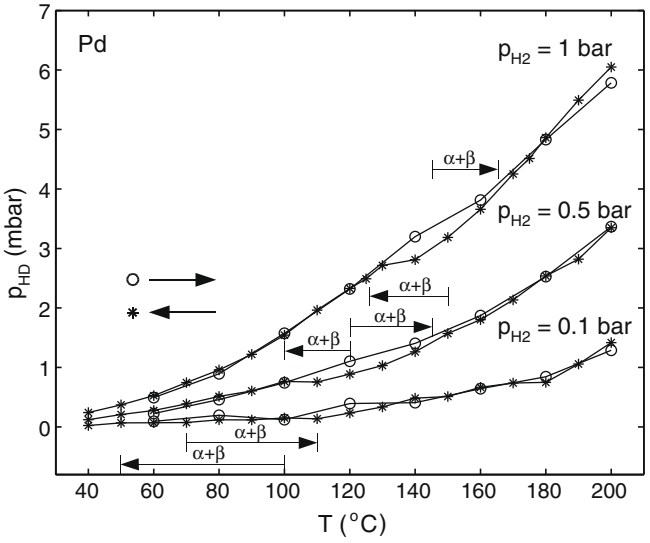

Fig. 4. The partial pressure of HD, p_{HD}, over the center of a Pd film as a function of temperature. The stars indicate data for decreasing and the circles for increasing temperature. The approximate temperature intervals where the α- and β-phases coexist during absorption and desorption are indicated for each pressure.

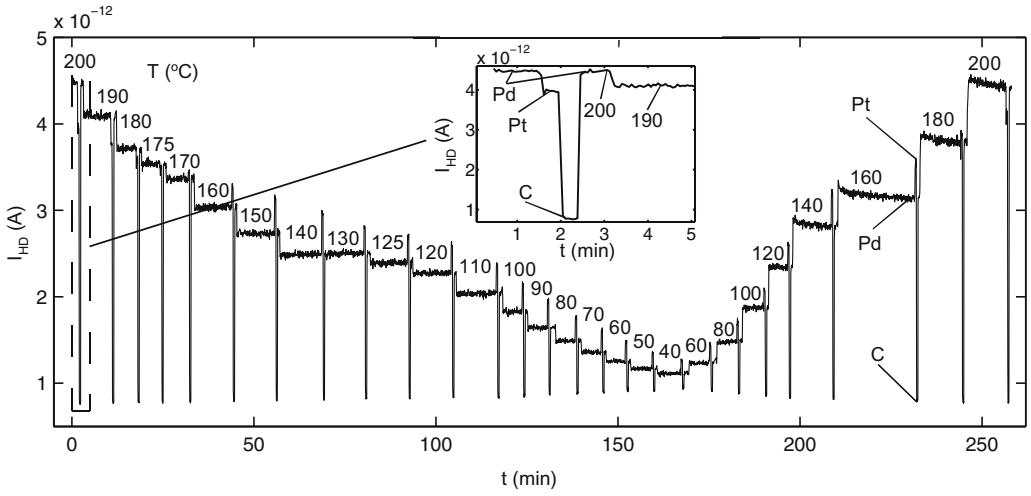

Fig. 3. The HD signal (3 AMU) as a function of time during a series of measurements in the high pressure cell. The gas sampling device is moved from a Pt to a Pd film and then to a clean area on the C substrate. After each cycle the temperature is changed.

3.1. The temperature range for the mixed $\alpha + \beta$-phase

It is well known that there is hysteresis for the hydrogen/Pd system as the pressure is cycled at a fixed temperature, so that the plateau pressure for absorption is higher than for desorption [22,23]. Such experiments are performed by measuring the hydrogen uptake and the steady-state pressure as a function of temperature. In order to identify the temperature region where the H/Pd system will go from α-phase to $\alpha + \beta$-phase and from $\alpha + \beta$-phase to β-phase in this experiment, which is performed at a constant pressure, it is necessary to analyze the published isotherms in some detail.

Fig. 5 shows desorption isotherms for the H/Pd system published by Frieske and Wicke [20]. Isotherms for both desorption and absorption have also been published by Lässer and Klatt [22]. The desorption isotherms correspond to thermodynamic equilibrium [23], and there is excellent agreement between the two data sets. The concentration limits for the mixed $\alpha + \beta$ region shown in Fig. 5 are the ones given by Frieske and Wicke [20]. Values for the lower concentration limit of the β-phase, which are in agreement with those given by Frieske and Wicke, were also published by Lässer and Klatt [22]. In the forthcoming, the phrase β-Pd will be used for β-phase Pd hydride, and α-Pd for α-phase solid solution of H in Pd.

In order to obtain values for the pressures investigated in this study, the following interpolation procedure was used for the isotherm data. First, interpolation was carried out to yield values for the pressure at a sufficient number of concentrations. By interpolation for a fixed concentration it is now possible to obtain the pressure at intermediate temperatures. Linear interpolation of the logarithm of the pressure was used throughout. By plotting a number of isotherms, as shown in Fig. 5, it is clear that the transition from α- to β-Pd will occur in the range 110–70 °C at 0.1 bar, 145–120 °C at 0.5 bar and 165–145 °C at 1 bar. These limits would be expected to be valid for desorption (increasing temperature) and are displayed in Table 1 and indicated in Fig. 4.

In order to predict the transition region for absorption (decreasing temperatures), the absorption isotherms by Lässer and Klatt are used [22]. Furthermore, it is assumed that the concentration limits

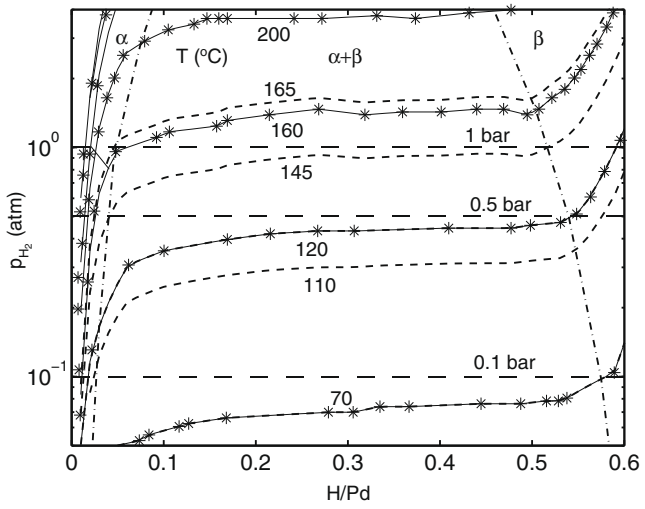

Fig. 5. The equilibrium pressure of hydrogen as a function of the bulk H/Pd ratio. The data points from Ref. [20] are denoted by stars. The limits for the transition from α to $\alpha + \beta$ and from $\alpha + \beta$ to β-phase are denoted by the dash-dotted curve and was also obtained from Ref. [20]. The solid curves are obtained by linear interpolation between the data points. The dashed curves are the interpolated isotherms for those temperatures where the isotherm cuts the lower or upper limit for the $\alpha + \beta$ region at 1, 0.5 and 0.1 bar.

Table 1
The upper temperature limit for the pure β-phase, $T_{\beta,max}$, and the lower temperature limit for the pure α-phase, $T_{\alpha,min}$. The values are approximate and were obtained from literature data as described in the text.

p (bar)	Absorption (decreasing T)		Desorption (increasing T)	
	$T_{\beta,max}$ (°C)	$T_{\alpha,min}$ (°C)	$T_{\beta,max}$ (°C)	$T_{\alpha,min}$ (°C)
0.1	50	100	70	110
0.5	100	120	120	145
1	125	150	145	165

for the mixed $\alpha + \beta$ region are the same as for the equilibrium isotherm. The interpolation was carried out as for the desorption isotherms. The approximate temperature limits for the mixed $\alpha + \beta$ region are displayed in Table 1 and indicated in Fig. 4. The values for 0.1 bar were obtained by extrapolation.

From Fig. 4, it can be seen that the predicted area of hysteresis agree very well with that seen experimentally, at least for 0.5 and 1 bar. Based on the shape of the curve for 1 bar, it is even tempting to assume that the data points below 140 °C for decreasing temperature are mainly β-Pd, and the ones above 140 °C for increasing temperature are mainly α-Pd. At 0.1 bar, the signal to noise ratio is worse as a consequence of the lower signal, and there is no clear hysteresis. This may be due to the fact that formation of hydride is too slow to be observed in this experiment at 80 °C.

The measurements by Lässer and Klatt were carried out on 10 μm thick Pd foil [22]. It has been reported that for Pd films with a thickness of less than 100 nm, the plateaus in the pressure versus uptake curves become less pronounced with decreasing film thickness [54–57]. Similar observations have also been made for nanoparticles with a diameter below approximately 10 nm [58–65]. In addition, the difference between the pressures for absorption and desorption in the pressure range where the α- and β-phases coexist for bulk Pd have been reported to vary with particle size [20,21,58,60,63–65]. One of the reasons for the change in the isotherms as compared to bulk Pd is that the hydrogen uptake in the α-phase is larger for nanoparticles [58,60–65]. This has been attributed to absorption of hydrogen in subsurface sites [58,60], to a strong increase in the heat of adsorption with decreasing particle size [61] or to an increase in the heat of formation for the β-phase [63]. It has also been argued that no phase transition occurs for particles with a diameter of 3.8 nm, whereas it does occur for particles with a diameter of 6 nm [66]. The picture is complicated by the fact that these studies report the total hydrogen uptake, i.e., it is not known how much of the hydrogen that was adsorbed on the surface. Later it was shown that for Pd particles with a diameter of about 10 nm supported on alumina, the bulk solubility for H in the α-phase is in fact higher than for bulk Pd [67]. The good agreement between the temperatures where hysteresis occurs in this measurement and the values predicted from bulk data actually indicates that, at least for the films studied here, hydrogen absorbed in the film bulk experiences the same environment as in bulk Pd.

The equilibrium pressure for a given concentration is significantly higher for D_2 than for H_2 [22]. This would lead to slightly lower concentrations (phase limits) at a given total pressure. Since the experiments in this study were carried out with only 1% D_2, the influence of D_2 on the isotherm is neglected.

3.2. The sticking probability

The sticking probability for H_2, S, at 1 bar can be obtained from the measured partial pressures of HD and D_2 by interpolation in calculated relations between S and the gas composition at the tip of the capillary. Fig. 6 shows the sticking probability extracted

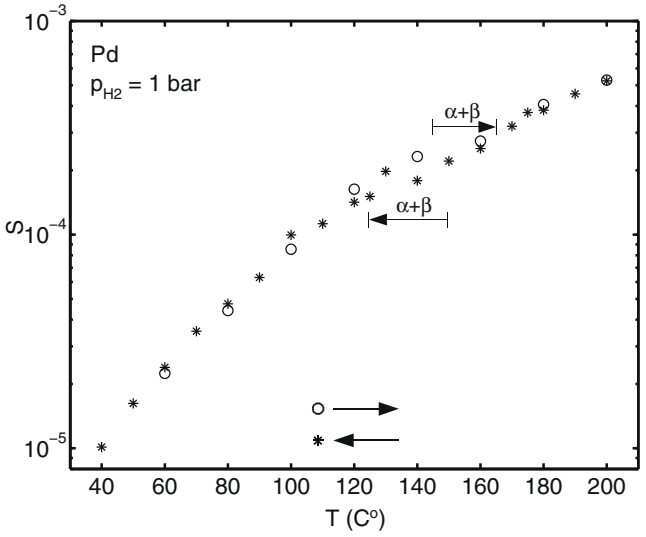

Fig. 6. The sticking probability for H_2, S, on Pd at 1 bar pressure. The temperature ranges where the α- and β-phases coexist during absorption and desorption are indicated in the figure.

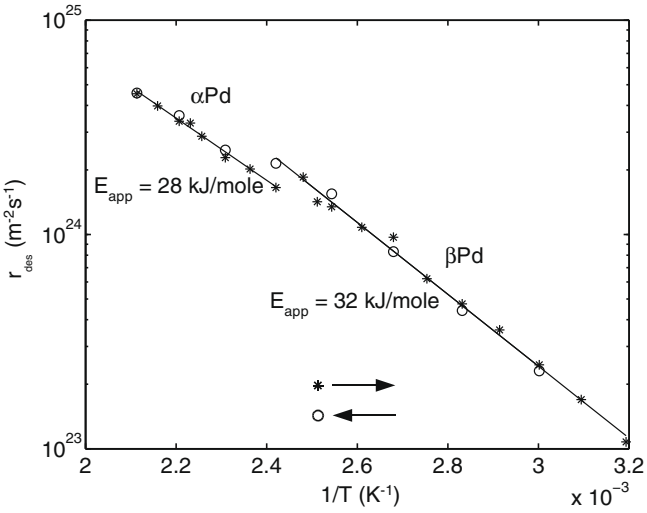

Fig. 7. Arrhenius plot for Pd at 1 bar. The prefactors, ξ, were 5.5×10^{27} s^{-1} m^{-2} and 2.6×10^{28} s^{-1} m^{-2} for α- and β-Pd, respectively.

from the data obtained at 1 bar along with the limits for the mixed $\alpha + \beta$ region.

No estimates for S could be obtained at pressures lower than one bar, since the rate of diffusion of HD against the direction of flow increases at lower total pressure, which makes it difficult to measure the correct background level over the graphite substrate. Also, the signal to background level is worse at lower pressure, since the leak rate of the capillary was optimized for 1 bar.

The dominating source of error in S is the uncertainty in the position of the capillary and nozzle relative to the sample. It is estimated that S can be measured with an accuracy of ±10% [51]. However, it was found that there is a difference in S between evaporations, probably caused by variations in the effective surface area, which gives rise to a variation in S of at most a factor of two [50]. It is therefore estimated, that the absolute magnitude of S is reliable within a factor of two, whereas the functional shape of S as a function of T should have a much smaller uncertainty, since the gas sampling device is not realigned during a series of measurements.

3.3. The apparent activation energy for desorption

With knowledge of the sticking probability, S, the adsorption rate for H_2 at 1 bar, r_{ads}, can be calculated according to

$$r_{ads} = SF_{H_2} \tag{5}$$

where F_{H_2} is the molecular flux of hydrogen toward the surface

$$F_{H_2} = \frac{p_{H_2}}{\sqrt{2\pi m_{H_2} kT}} \tag{6}$$

Here, p_{H_2} is the hydrogen pressure and m_{H_2} the molecular mass of H_2.

Since, in steady state,

$$r_{ads} = r_{des} \tag{7}$$

the apparent activation energy for desorption, E_{app}, can be obtained by fitting the logarithm of the expression

$$r_{des} = \xi \exp\left(\frac{-E_{app}}{kT}\right) \tag{8}$$

to an Arrhenius plot of r_{des}, as is shown in Fig. 7. Note that the prefactor ξ and E_{app} are assumed to be temperature independent in Eq. (8). In the Arrhenius plots, the data points below 140 °C for decreasing temperature are ascribed to β-Pd, and the ones above 140 °C for increasing temperature are ascribed to α-Pd.

Table 2 contains average values for E_{app} and ξ, $\overline{E_{app}}$ and $\bar{\xi}$, obtained in a number of experiments. In addition to the high temperature resolution experiments like the one shown in Fig. 7, also data from experiments with lower temperature resolution are reported. In a low temperature resolution experiment, measurements were carried out for the temperatures 200, 175, 150, 125, 100, 80, 60, 40, 150 and 200 °C. In such an experiment there are thus only three temperature points in the α-Pd region.

In order to be able to compare the apparent energies of desorption, E_{app}, to calculated and measured values for the desorption energy, E_{des}, it is assumed that the rate of desorption is given by the mean field expression

$$r_{H_2} = \frac{1}{2} \nu_{H_2} \theta_H^2 N_s \exp\left(\frac{-E_{des}(\theta_H)}{kT}\right) \tag{9}$$

By comparing with Eq. (8), it follows that

$$\xi = \frac{1}{2} \nu_{H_2} \theta_H^2 N_s \tag{10}$$

There seems to be no information available in the literature on θ_H as a function of the temperature at a hydrogen pressure of 1 bar. However, the low values obtained for the sticking probability indicate that the surface has a high coverage of H. Thus, the sticking probability at $\theta_H = 0$, S_0, has been shown to be 0.1–0.2 for Pd(1 1 1) [18] and to drop at least a factor of 100 when θ_H increases to 1 [13]. For Pd(1 0 0) it is reported that $S = 0.017$ for $\theta_H = 1.3$ [14]. Hence, it is assumed that the $\theta_H \approx 1$, so that θ_H can be assumed to be a weak function of the temperature in Eq. (10). A related problem is, that in order for E_{des} to be comparable to E_{app}, E_{des} must be reasonably constant over the (small) variation in θ_H that occurs over the temperature range investigated. As will be discussed further on, the DFT calculations indicate that the activation energy for desorption is not strongly coverage dependent, at least not for the (1 1 1) surfaces of Pd and Pd hydride and $\theta_H \leqslant 1$. The values for ν_{H_2} displayed in Table 2 were calculated from Eq. (10), under the assumptions that $\theta_H = 1$, and that ν_{H_2} is independent of temperature.

The value of approximately 30 kJ/mole H_2 obtained for E_{app} for β-Pd in this study is in excellent agreement with the value reported for E_{des} for β-Pd of 33.8 kJ/mole H_2 [28]. Another study, where no surface analysis was carried out, gives similar values for E_{des} if

Table 2
Average values and standard deviations for E_{app} and ξ. The table also contains values for ν_{H_2} calculated from ξ under the assumption that $\theta_H = 1$ and that the site density is equal to the atomic density of the close packed surface, N_s. N is the number of experiments used for the analysis. Experiments with low temperature resolution are indicated by LR and experiments with high temperature resolution by HR. The low resolution data obtained for $T < 150$ °C was reported previously [51].

	$\overline{E_{app}}$ (kJ/mole H_2)	Std (E_{app}) (kJ/mole H_2)	$\bar{\xi}$ ($m^{-2}\,s^{-1}$)	Std (ξ) ($m^{-2}\,s^{-1}$)	N_s (m^{-2})	$\overline{\nu_{H_2}}$ (s^{-1})	N
α-Pd, LR	29.7	1.8	1.22×10^{28}	4.5×10^{27}	1.5×10^{19}	1×10^{9}	9
β-Pd, LR	29.3	1.9	1.49×10^{28}	6.0×10^{27}	1.4×10^{19}	1×10^{9}	9
α-Pd, HR	29.3	2.1	6.50×10^{27}	1.41×10^{27}	1.5×10^{19}	4×10^{8}	2
β-Pd, HR	31.6	0.3	1.90×10^{28}	9.90×10^{27}	1.4×10^{19}	1×10^{9}	2

the evaluation principle used in Ref. [28] is applied to the data for β-Pd [68].

In contrast, for α-Pd it is reported that the heat of adsorption for the highest θ_H achieved under vacuum conditions is 75 kJ/mole for Pd(1 1 0) [18], 71 kJ/mole for Pd(1 0 0) [14] and 100 kJ/mole for a Field Emission Microscopy (FEM) tip [8]. In addition, it was deduced that $E_{des} = 78$ kJ/mole H_2 at $\theta_H = 0.9$ for Pd(1 1 1) under the assumption of a second order sticking probability [13]. Since the pressure of 1 bar used here is at least seven orders of magnitude higher than in the vacuum studies, a higher θ_H, and consequently a lower heat of adsorption would be expected. However, even if it is assumed that there is no barrier for adsorption, the values obtained under vacuum conditions are much higher than the value of approximately 29.5 kJ/mole H_2 obtained for E_{app} for α-Pd in this study. As a matter of fact, an earlier study showed that the agreement between E_{app} and the heat of adsorption measured under vacuum conditions at high coverage is significantly better for the metals Ni, Co, Rh, Ru, Ir and Pt than for Pd [50]. The main reason for the discrepancy is probably that, in general, true equilibrium between bulk and surface is not achieved in vacuum experiments, due to the high solubility and the slow diffusion of H in Pd at typical dosing temperatures [13,18,19]. Thus, it is expected to be difficult to populate adsorption sites with a low heat of adsorption under vacuum conditions, since H will tend to go into the bulk instead.

Since the value obtained for E_{app} for α-Pd of 29.5 kJ/mole H_2 is still higher than the heat of absorption in the Pd bulk (19 kJ/mole H_2), it would be expected that the surface coverage of H is significantly higher than the bulk concentration, if it is assumed that adsorption is unactivated and E_{app} is an effective value for the most loosely bound hydrogen on the surface. This is confirmed by the low values for S measured for α-Pd which indicate that $\theta_H \approx 1$ while the bulk is still in the low concentration α-phase.

In order to compare r_{des} for α- and β-Pd, r_{des} was calculated for 140 °C with the help of Eq. (8) and the values for E_{app} and ξ for α and β-Pd, respectively. From the values for r_{des}, the ratio $Q_{140} = r_{des,\beta}(140)/r_{des,\alpha}(140)$ was calculated. If all the measurements, including the ones with low temperature resolution, are used, the average value for Q_{140}, $\overline{Q_{140}}$, over 11 measurements is 1.36 with a standard deviation of 0.11. From Eqs. (5) and (7) it also holds that $Q_{140} = S_{\beta(140)}/S_{\alpha(140)}$. Note that it is obvious from Fig. 6 that S is higher for β-Pd than for α-Pd, and that this conclusion is not dependent on the extraction procedure used for E_{app}. In the context of S, the use of Eq. (8) to calculate $S_{\beta(140)}/S_{\alpha(140)}$ can be considered as an interpolation procedure which is used to increase the accuracy.

Based on the standard deviation for E_{app} in Table 2, it seems reasonable to estimate the error in E_{app} to ±2 kJ/mole for both α-Pd and β-Pd. The larger standard deviation for ξ in Table 2 is believed to be a consequence of the variation in microscopic surface area between different measurements [50].

The values for ν_{H_2} in Table 2 are much lower than expected from transition state theory. The reason for this is presently not understood, but a discussion on the topic may be found in Ref. [50].

3.4. The influence of C

It has been reported that C is absorbed in the Pd bulk during hydrogenation reactions [4,6,7], and that such absorbed C influences the adsorption energy for H [7]. Even though it is not obvious that graphite would give rise to absorbed C under the conditions encountered in this study, it cannot be excluded that C is present on the Pd surface and this could influence the activation energy for desorption of hydrogen. In order to investigate whether C on the surface or in the Pd bulk influenced the measured values for S, experiments were performed with 1000 Å thick Pd films evaporated on freshly cleaved, unsputtered HOPG. From analysis with XPS, which was added to the setup after the completion of the main series of experiments, it is concluded that for these films, the amount of C on the Pd surface is below the detection limit (1%) both before and after the high pressure measurements. Unfortunately, for these thick films, the approach to steady state is very slow (several hours) close to the temperature range where the α- and β-phase coexist, and therefore it was not possible to measure S in the range $100 < T < 160$. However, the values for S measured for pure α-Pd and β-Pd agree, within the accuracy of the experiment, with the values obtained for the 50 Å films.

4. DFT calculations

4.1. Model and calculational details

In order to describe the experiments presented in this paper, a model system for β-phase Pd hydride was developed. For the α-phase solid solution of H in Pd, the pure Pd metal is used as a model for the α-phase bulk, since it would require prohibitively large unit cells to model systems with H bulk concentrations well below 5%, see Fig. 5. Adsorption of H was studied on both the Pd(1 1 1) and the Pd(2 1 1) surfaces in order to elucidate the influence of steps.

The neglect of bulk H in the model for the α-phase can be justified by the good general agreement between DFT calculations where bulk H is not taken into account, and experiments performed under UHV conditions, where bulk H is always present to some degree, see e.g. Refs. [9–13,19]. The experimental studies of most relevance for this investigation are the ones with the highest H surface coverage (and thus H bulk concentration). As mentioned in Section 3.3, values for the heat of adsorption and the desorption energy in the interval 71-78 kJ/mole H_2 have been reported for low index surfaces of Pd at hydrogen coverages close to saturation [13,14,18]. This is in reasonable agreement with the value for the integral adsorption energy of 75 kJ/mole H_2, obtained in a DFT study of H adsorption on Pd(1 1 1) where bulk H was not taken into account [38]. Furthermore, the results of another DFT study indicate that the interaction between subsurface H and H adsorbed in the fcc-hollow site is weak [37].

All calculations are carried out using self-consistent DFT calculations with the Dacapo code [69], which uses plane waves as the ba-

sis set for the Kohn–Sham wave functions [70,71], and Vanderbilt ultra-soft pseudo-potentials to represent the ionic cores [72]. The GGA-RPBE exchange-correlation functional is used in all calculations [73]. The energy cut-off of the plane waves and the density are both chosen to be 26 Ry (354 eV). The calculations on the Pd(1 1 1) and Pd hydride slabs are performed in periodically repeated 2×2 and 4×4 unit cells with three layers of Pd, with $4 \times 4 \times 1$ and $2 \times 2 \times 1$ Monkhorst Pack *k*-point sampling, respectively. The large unit cells are necessary for calculations with H coverages close to 1 ML, for reasons which will be explained in the results section. The Pd(2 1 1) step has three layers underneath the step and a 2×3 unit cell with 4×4 *k*-points sampling. The slabs are separated with circa 12 Å vacuum to prevent interaction between images. The number of Pd-layers, *k*-point sampling and vacuum distance have all been evaluated in test systems and found to be high enough to ensure convergence in the total energies.

In the model for Pd hydride, the H/Pd ratio in the bulk is assumed to be 0.75. This H/Pd ratio was found to give the lowest energy for H/Pd ratios between zero and one [5]. Different configurations were calculated for this bulk concentration with three layers of Pd and 1 ML of H adsorbed on the HCP hollow sites on the surface. The configuration with 1.0 H/Pd in the bottom octahedral holes and 0.5 H/Pd in the top octahedral holes was found to yield the lowest energy and was used in the Pd hydride model. The lattice constant for Pd bulk was optimized with the RPBE functional to be 4.02 Å. Optimization of the lattice constant for the hydride using the RPBE functional resulted in a value of 4.15 Å, which is a 3.2% expansion from the pure Pd slab [5]. This is in excellent agreement with experimentally determined values of 3.3% [26] and 3.47% [27]. For the Pd(1 1 1), Pd(2 1 1) and the Pd hydride slabs the two bottom Pd layers are frozen but the atoms in the top Pd layer are allowed to move. The subsurface H in the bulk as well as the H adsorbed on the surface are allowed to relax. The Pd hydride slab with a H/Pd ratio of 0.75 in the bulk and 1 ML of H adsorbed in the hcp holes on the surface is shown in Fig. 8, together with the Pd(2 1 1) slab.

The influence on the results caused by inclusion of the zero point energy (ZPE) was also studied. The ZPE was calculated using normal mode analysis with DFT calculations for the Pd(1 1 1) and the Pd hydride surface. The ZPE for H_2 in the gas phase is 26.1 kJ/mole per H_2 [74]. For the H adsorption state, values of 31.8 kJ/mole per $2H^*$ for Pd and 30.9 kJ/mole per $2H^*$ for Pd hydride were found. The calculated ZPE for the transition state was 29.9 kJ/mole per $2H^{TS}$ for Pd and 26.1 kJ/mole per $2H^{TS}$ for Pd hydride. The difference in binding energy between Pd and Pd hydride will thus only change by 1.0 kJ/mole H_2 if the ZPE is included. The difference between the activation energies for Pd and Pd hydride changes by 3.9 kJ/mole H_2 when the ZPE correction is taken into account. These differences are small compared to the accuracy of the calculations, and will not influence the conclusions drawn in this paper. Hence, all energies are reported without the ZPE correction.

4.2. Results

4.2.1. The differential adsorption energy

The binding energies for H atoms on different sites on the Pd(1 1 1), Pd(2 1 1) and Pd hydride slabs are calculated relative to H_2 molecules in the gas phase. The high symmetry sites fcc, hcp,

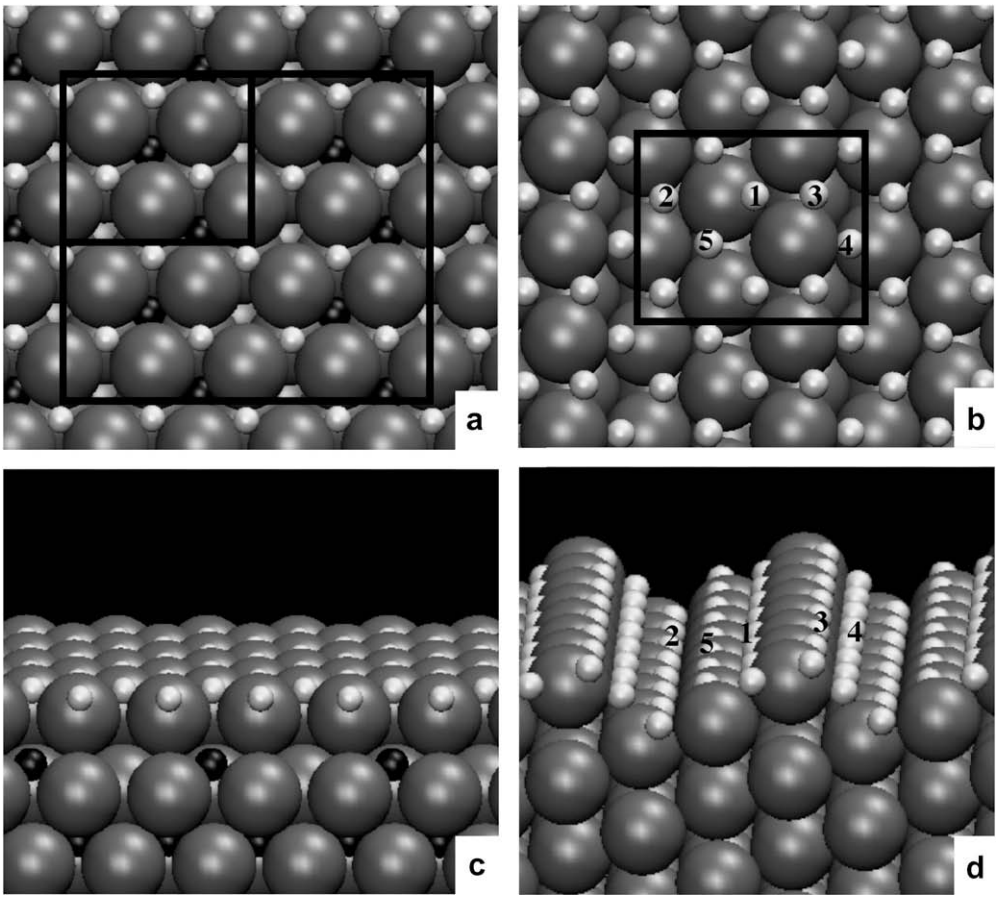

Fig. 8. (a) Top view and (b) tilted side view of the Pd hydride structure with the three Pd-layers (grey) and the two subsurface H-layers (black). One monolayer of H is adsorbed in the hcp sites on the surface (light grey). (c) Top view and (d) tilted side view of the Pd(2 1 1) stepped surface. The H adsorbed on the surface are numbered in order of decreasing binding strength. The dimensions of the unit cells used are indicated for both surfaces.

bridge and on-top were considered. For the Pd(1 1 1) surface, the fcc sites are the most stable, as expected for a (1 1 1) facet of an fcc crystal. However, the hcp-hollow sites were found to be the most stable for the hydride surface, indicating a significant repulsion from the H-atom just below the fcc-hollow site. For the Pd(2 1 1) surface, H binds strongest to the fcc sites at the step for the coverages 1/6–2/6 ML in our model (H labeled 1 in Fig. 8). For 3/6–4/6 ML coverage, H additionally occupies the fcc hollow sites on the (1 1 1) microfacet (H labeled 2) and for coverages of 5/6–6/6 ML, the bridge sites on the step are occupied (labeled 3). At higher H coverage, H binds to the bridge site of the (1 0 0)-like site underneath the step (labeled 4) and the last H considered here bind to hollow sites on the microfacet (labeled 5). This behavior is quite different from the results of exactly the same kind of DFT calculations for the Pt(2 1 1) surface, where H is initially adsorbed at the step and thereafter occupies the (1 1 1) microfacet [75].

Fig. 9 shows the differential adsorption energy for H on the fcc site on Pd(1 1 1) and in the hcp site on Pd hydride as a function of H surface coverage up to 1 ML. For Pd(2 1 1), various sites are occupied as the coverage increases, as mentioned above. The initial adsorption energy (low H coverage) is calculated to be −81 kJ/mole H_2 for the Pd(1 1 1) slab. This is in reasonable agreement with the experimental value for the heat of adsorption at low H coverage on the Pd(1 1 1) surface of 90 kJ/mole H_2 [18]. Published calculated values for the adsorption energy for H at low coverage on Pd(1 1 1) fall in the range −133 to −85 kJ/mole H_2 [30,31,34,38–41]. In one of these studies H was found to bind strongest to the hcp site [34]. According to our calculations, the initial adsorption energy for H on Pd(2 1 1) is very close to that for Pd(1 1 1), in agreement with a previous theoretical study on Pd(2 1 1) [41]. We have not found any experimental values for the heat of adsorption for H on the Pd(2 1 1) surface.

It is assumed that the system having 1 ML of H on the surface describes the conditions of the experiments. As can be seen from Fig. 9, the differential adsorption energy increases when approaching 1 ML H coverage. The differential adsorption energy at 1 ML H is −50.9 and −38.6 kJ/mole H_2 for the Pd(1 1 1) and the Pd hydride surface, respectively. The mean absolute error compared to experiments in the differential adsorption energy should be less than 25 kJ/mole H_2 [73], but the relative error between the two systems should be much smaller. We have not found any experimental data to compare these values to.

Several configurations were considered for H coverages above 1 ML on both surfaces. For a (1 1 1) fcc crystal surface with 1 ML in fcc sites, the next H prefer to bind to the on-top sites rather than to the hcp sites [76]. For the Pd hydride surface, however, H on the fcc sites are more stable than H on the on-top sites. Fig. 9 shows the calculated binding energy for the fcc/on-top sites for Pd(1 1 1) and for the hcp/fcc sites for Pd hydride above 1 ML. In both cases it is unfavorable to adsorb H above 1 ML with respect to H_2 in the gas phase. However, it is two times more unfavorable to put additional H on the on-top sites of the Pd(1 1 1) slab than on the fcc sites of the Pd hydride slab. In order to get a data point just above 1 ML and to see this discontinuity in the differential adsorption energy, larger unit cells, 4×4, are used with 17/16 ML H coverage. Going beyond 1 ML does not, however, cost as much energy on the Pd(2 1 1) surface as on the Pd(1 1 1), since more alternative binding sites are available around the step. A higher coverage than 1 ML can thus be expected for a surface with defects. Since a polycrystalline Pd surface was used in this study, the Pd(2 1 1) model system would be expected to give a better description of the heat of adsorption.

4.2.2. Activation barriers for adsorption and desorption

In order to study the kinetics of H_2 adsorption and desorption the activation barriers, E_a, were calculated with the Nudged Elastic Band (NEB) method [77,78]. The calculated barriers for dissociation and recombination at different H coverages are shown in Fig. 10.

The activation energy for desorption:

The desorption barrier for H_2 on Pd(1 1 1) and Pd hydride is quite high (around 65–82 kJ/mole H_2) and rather constant up to 1 ML, but above 1 ML, the activation energy decreases. At 1 ML, the desorption barrier on the Pd hydride surface is slightly lower, 65.3 kJ/mole H_2, than on the Pd(1 1 1) surface, 75.8 kJ/mole H_2. For Pd(1 1 1), values for the activation energy for desorption at $\theta_H = 1$ of 63 kJ/mole H_2 [10] and 78 kJ/mole H_2 [13] were obtained by fitting models to experimental data. The agreement between experiment and theory must, however, be viewed with caution considering the assumptions used when extracting the activation energies from experimental data.

Comparing the absolute magnitude of these desorption barriers with the value found in the experiments of this paper, the DFT calculations are more than two times higher. The apparent desorption energy for α-Pd given in Table 2 is about 29.5 kJ/mole H_2 and the calculated barrier 75.8 kJ/mole H_2 for the Pd(1 1 1) model system at 1 ML coverage. Since the surfaces studied in the experiment are very rough and most likely have high concentrations of defects and steps, NEB calculations were carried out for the Pd(2 1 1) model

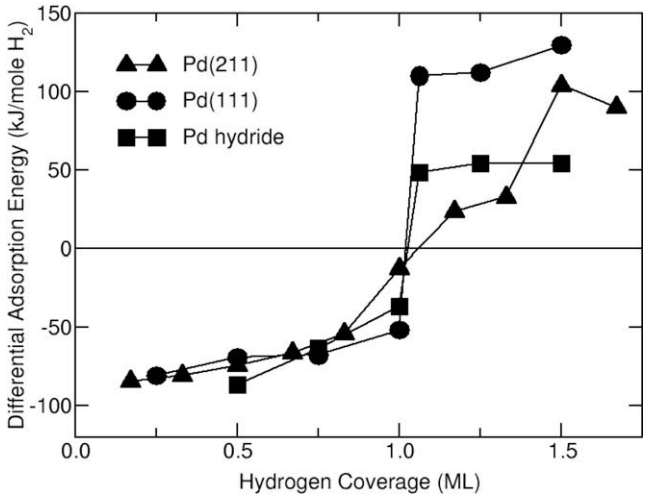

Fig. 9. Differential adsorption energy for H as a function of the surface H coverage on Pd(1 1 1), Pd(2 1 1) and Pd hydride slabs.

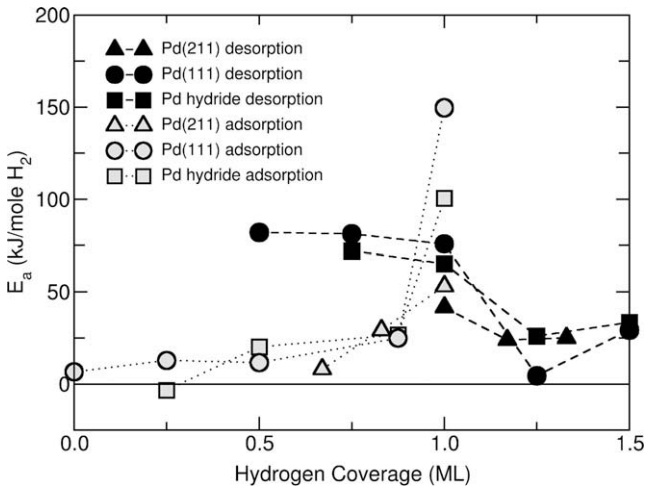

Fig. 10. Activation energy, E_a, for adsorbing (open symbols) and desorbing (filled symbols) H_2 as a function of initial H coverage on Pd(1 1 1) (circles), Pd(2 1 1) (triangles) and Pd hydride (squares) slabs.

system with 1.00, 1.17 and 1.33 ML initial H coverage. The desorption barriers thus obtained of 41.6, 24.0 and 25.1 kJ/mole H_2, respectively, are in very good agreement with our experimental value of 29.5 kJ/mole H_2. It is likely that steps would have a similar effect on the activation energy for Pd hydride, since the desorption barriers were very similar on the (1 1 1) surfaces of Pd and Pd hydride.

The activation energy for adsorption:

The activation barrier for H_2 adsorption increases slightly with H coverage (−3 to 27 kJ/mole H_2) on Pd(1 1 1) and Pd hydride below 1 ML. Previous theoretical studies all report non-activated dissociation on Pd [33,40,47]. Here we get a 6.6 kJ/mole H_2 adsorption barrier on the clean Pd(1 1 1) slab. The reason for the slightly positive adsorption barrier (instead of zero or negative barrier when comparing it to H_2 in the gas phase) is the use of the RPBE xc-functional, whereas in the previous studies the PW91 functional, see Ref. [79], was used [33,40,47]. The latter functional over binds adsorbed H, whereas the RPBE functional tends to give slightly too low predictions for H adsorption energies when compared to experimental values [50]. When using the PW91 xc-functional a value of −5 kJ/mole H_2 is obtained for the activation energy for adsorption on the clean Pd(1 1 1) surface which is in better agreement with the value of −21 kJ/mole H_2 calculated by Lopez et al. with PW91 for a clean Pd(1 1 1) surface [40].

In order to get closer to 1 ML, the unit cell size is increased from 2×2 to 4×4. Thus one H_2 molecule is adsorbed on a surface with 14/16 ML H coverage, resulting in 16/16 ML H coverage. This is adsorption to a dimer vacancy. The vacancy aggregation energy, or the energy required to create dimers from isolated vacancies, is found to be rather small, 0.07 eV, and the lifetime of those dimers is relatively long [40]. If an H_2 molecule is adsorbed onto the surface and the H coverage becomes higher than 1 ML in the final state, the activation energy becomes much higher since the adsorption sites occupied are very unstable, as can be seen from Fig. 9. This can also be seen in Fig. 10, where having initially 1 ML H and adsorbing one H_2, obtaining a final coverage of 1.5 ML, results in activation barriers of 150 and 101 kJ/mole H_2 for the Pd(1 1 1) and the Pd hydride surfaces, respectively.

The system best describing the experimental conditions here would be the one having 14/16 ML coverage in the 4×4 unit cells. The barriers are 24.9 kJ/mole H_2 for Pd(1 1 1) and 26.7 kJ/mole H_2 for the Pd hydride surface. Using the PW91 xc-functional for the Pd(1 1 1) surface a barrier of −8 kJ/mole H_2 is obtained. This is in agreement with other PW91 calculations at similar H coverage, where dissociation barriers of zero for a dimer vacancy, −3.9 kJ/mole H_2 for a triple vacancy centered around a hollow site and −11.6 kJ/mole H_2 for a triple vacancy centered around a top site were obtained [40].

In the experimental literature, adsorption of H_2 on clean Pd surfaces is in general considered to be unactivated, since it occurs with a high probability (>0.1) also at low temperatures [12,14,18,19]. Molecular beam studies on Pd(1 1 1), Pd(1 1 0) and Pd(1 0 0) reveal both activated and unactivated adsorption paths [16,17]. The barrier for adsorption of H_2 on Pd(1 1 1) via the activated path is estimated to be 4.8 kJ/mole H_2 [16]. A molecular beam study where H coverages up to 0.9 were studied gave no indication of a barrier for adsorption [13].

Presently, it is not clear whether the discrepancy between the calculations of the activation energy for adsorption for the Pd(1 1 1) surface and the experimental data from the literature data is due to the calculations overestimating the activation energy for adsorption, or if it is due to the experiments being influenced by the inevitable defects and steps present on real single crystal surfaces. The calculations for Pd(2 1 1) confirm that the presence of steps on the surface may lead to a significant decrease in the activation energy for adsorption. Hence, it is presently an open question whether there is a barrier for adsorption at high H coverage on the polycrystalline Pd surfaces studied here.

5. Discussion

The agreement between the temperature range where hysteresis occurs in our experiments and that predicted from literature data is a strong indication that, at least for pressures above 0.1 bar, the phase transition between α-Pd and β-Pd actually occurs under these experimental conditions. The slow attainment of steady state seen close to the temperature region where the hysteresis occurs is additional evidence that the phase transition takes place, since it is well known that the rate of formation/destruction of β-Pd may be extremely slow for bulk samples [53]. This is also illustrated by the dramatic increase in the time needed to reach steady state for the 1000 Å thick Pd films as compared to the 50 Å thick films. Based on these observations it is concluded that at 1 bar hydrogen pressure, the data points below 140 °C corresponds to β-Pd, and the ones above 140 °C to α-Pd.

The observed differences in the rate of hydrogen splitting between α- and β-Pd are rather small. At the temperature where α- and β-Pd coexist, 140 °C, the adsorption/desorption rate for H_2 on β-Pd is approximately 1.4 times higher than that on α-Pd. Assuming all other factors equal, this corresponds to a difference in activation energy of 1 kJ/mole H_2 at 140 °C, which is significantly smaller than the uncertainty in both DFT calculations and the extraction of E_{app}.

Keeping the limited accuracy of the calculations and measurements in mind, it is nevertheless interesting to see how much of the difference in S between α- and β-Pd that can be explained. The low sticking probabilities measured indicate that the surfaces are close to saturated at all temperatures studied here. From Fig. 9, the difference in the differential adsorption energy between Pd hydride and Pd(1 1 1) is about 12 kJ/mole H_2 at 1 ML H coverage. Based on the result for the (1 1 1) surfaces, it seems likely that H binds less strongly to Pd hydride than to Pd. A lower heat of adsorption for H on β- than on α-Pd would be expected to lead to a slightly lower equilibrium coverage of H on β-Pd, which would be expected to give a higher value for S, in agreement with what is observed in the experiments.

The Pd(2 1 1) surface is expected to be the most suitable of the investigated model systems for studies of the activation energies for adsorption and desorption for the polycrystalline Pd surfaces used in the experiments. The calculated activation energy for desorption at 1 ML H coverage of 42 kJ/mole H_2 for Pd(2 1 1) is in reasonable agreement with the experimentally obtained values for E_{app} for α-Pd of close to 30 kJ/mole H_2. Experimentally, it is found that E_{app} is the same for α- and β-Pd within 4 kJ/mole H_2. The calculated activation energy for desorption is slightly smaller for Pd hydride than for Pd(1 1 1), as can be seen in Fig. 10. However, the difference has to be considered to be within the margin of uncertainty.

Fig. 11 shows calculated energy diagrams for adsorption and desorption of H_2 on Pd(2 1 1), Pd(1 1 1) and Pd hydride. The final H coverage is 1 ML, except for the trimer vacancies where the final coverage is 0.75. The diagram was obtained from the data presented in Fig. 10. As can be seen from Fig. 11, the local arrangement of the adsorbed H on the surface is important for the activation energy for adsorption, as already seen elsewhere for the Pd(1 1 1) surface [40,46,47]. It should be noted that the energy level for the adsorbed state is the integral and not the differential adsorption energy.

The activation energy for adsorption varies between 0 and 25 kJ/mole H_2, depending on surface and H configuration on the surface. As a matter of fact, adsorption on a trimer vacancy on Pd

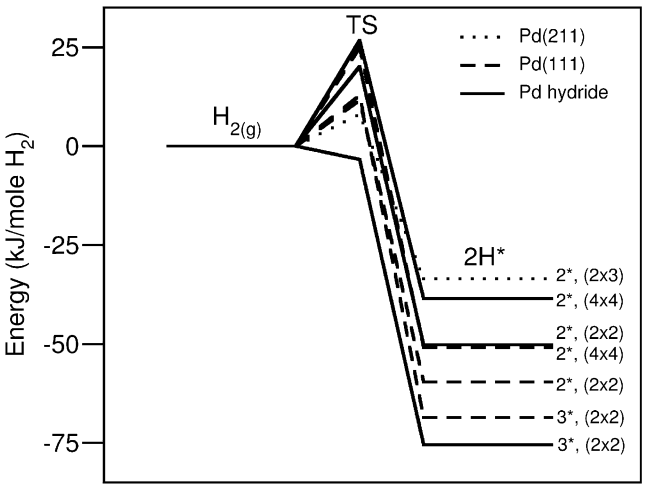

Fig. 11. Energy diagram for adsorbing and desorbing H_2 on Pd(1 1 1), Pd(2 1 1) and Pd hydride surfaces. The labels 2* and 3* denote adsorption on dimer and trimer vacancies, respectively. The numbers within parenthesis give the size of the unit cell used in the calculations. The H coverage is 1 ML for 2* and 0.75 ML for 3*.

hydride is seen to occur without a barrier for adsorption, whereas there is always a barrier for adsorption on the Pd surfaces. This would of course immediately explain why S is higher for β- than for α-Pd. Considering the discrepancies with experiments as to whether there actually is a barrier for adsorption at high coverage on Pd(1 1 1), and the possibility that the barrier for adsorption would be lower on a polycrystalline Pd surface, it is only concluded that the activation energy for adsorption on β-Pd is similar to the one on α-Pd.

The effect of the difference in H_2 dissociation rate between α- and β-Pd on the overall rate of, e.g., a hydrogenation reaction will depend on the extent to which hydrogen splitting is rate limiting for the overall reaction. However, since it seems likely that the H coverage on β-Pd is slightly lower than on α-Pd under identical conditions, it could be expected quite generally that for a reaction where the rate is limited by a high H coverage, the rate would increase slightly as β-Pd is formed in the bulk. It should be noted that under reaction conditions the H concentration in the Pd bulk is determined by the steady state H coverage on the surface, rather than by the partial pressure of hydrogen over the catalyst. Also, the binding energy of H on the surface will in general be influenced by co-adsorbates other than H as well as by the state of the Pd bulk.

6. Conclusions

Adsorption and desorption of H_2 at 1 bar pressure is faster on β- than on α-Pd. The most likely explanation for the difference in rate is that hydrogen binds weaker to β- than to α-Pd, which gives rise to a somewhat lower H equilibrium coverage on β-Pd, which in turn results in a slightly higher dissociative sticking coefficient for H_2 on β-Pd.

Acknowledgment

Center for Individual Nanoparticle Functionality (CINF) is sponsored by The Danish National Research Foundation.

References

[1] G. Rupprechter, G.A. Somorjai, Cat. Lett. 48 (1997) 17.
[2] P.A. Sheth, M. Neurock, C.M. Smith, J. Phys. Chem. B 107 (2003) 2009.
[3] A.M. Doyle, S.K. Shaikhutdinov, S.D. Jackson, H.-J. Freund, Angew. Chem. Int. Ed. 42 (2003) 5240.
[4] D. Teschner, J. Borsodi, A. Wootsch, Z. Revay, M. Hävecker, A. Knop-Gericke, S.D. Jackson, R. Schlögl, Science 320 (2008) 86.
[5] F. Studt, F. Abild-Pedersen, T. Bligaard, R.Z. Sørensen, C.H. Christensen, J.K. Nørskov, Angew. Chem. Int. Ed. 47 (2008) 9299.
[6] M. Wilde, K. Fukutani, W. Ludwig, B. Brandt, J.-H. Fischer, S. Schauermann, H.-J. Freund, Angew. Chem. Int. Ed. 47 (2008) 9289.
[7] D. Teschner, Z. Revay, J. Borsodi, M. Hävecker, A. Knop-Gericke, R. Schlögl, D. Milroy, S.D. Jackson, D. Torres, P. Sautet, Angew. Chem. Int. Ed. 47 (2008) 9274.
[8] P.D. Cobden, B.E. Nieuwenhuys, V.V. Gorodetskii, Appl. Cat. A 188 (1999) 69.
[9] G.E. Gdowski, T.E. Felter, R.H. Stulen, Surf. Sci. 181 (1987) L147.
[10] I. Ratajczykowa, Surf. Sci. 172 (1986) 691.
[11] H. Okuyama, W. Siga, N. Takagi, M. Nishijima, T. Aruga, Surf. Sci. 401 (1998) 344.
[12] M.G. Cattania, V. Penka, R.J. Behm, K. Christmann, G. Ertl, Surf. Sci. 126 (1983) 382.
[13] T. Engel, H. Kuipers, Surf. Sci. 90 (1979) 162.
[14] R.J. Behm, K. Christmann, G. Ertl, Surf. Sci. 99 (1980) 320.
[15] J. Fogelberg, M. Eriksson, H. Dannetun, L.-G. Peterson, J. Appl. Phys. 78 (1995) 988.
[16] Ch. Resch, H.F. Berger, K.F. Rendulic, E. Bertel, Surf. Sci. 316 (1994) L1105.
[17] K.D. Rendulic, G. Anger, A. Winkler, Surf. Sci. 208 (1989) 404.
[18] H. Conrad, G. Ertl, E.E. Latta, Surf. Sci. 41 (1974) 435.
[19] U. Muschiol, P.K. Schmidt, K. Christmann, Surf. Sci. 395 (1998) 182.
[20] H. Frieske, E. Wicke, Ber. Bunsenges. Phys. Chem. 77 (1973) 48.
[21] E. Wicke, G.H. Nernst, Ber. Bunsenges. Phys. Chem. 68 (1964) 224.
[22] R. Lässer, K.-H. Klatt, Phys. Rev. B 28 (1983) 748.
[23] E. Wicke, J. Blaurock, J. Less Common Metals 130 (1987) 351.
[24] R. Lässer, G.L. Powell, Phys. Rev. B 34 (1986) 578.
[25] W.C. Chen, B.J. Heuser, J. Alloys Comp. 312 (2000) 176.
[26] E. Wicke, H. Brodowski, in: G. Alefeld, J. Völkl (Eds.), Hydrogen in Metals II, Springer, Berlin, 1978.
[27] M. Hansen, Constitution of Binary Alloys, McGraw-Hill, New York, 1958. pp. 790–793.
[28] P.A. Bennet, J.C. Fuggle, Phys. Rev. B 26 (1982) 6030.
[29] D. Tománek, Z. Sun, S.G. Louie, Phys. Rev. B 43 (1991) 4699.
[30] J.-F. Paul, P. Sautet, Phys. Rev. B 53 (1996) 8015.
[31] W. Dong, G. Kresse, J. Furthmüller, J. Hafner, Phys. Rev. B 54 (1996) 2157.
[32] J.-F. Paul, P. Sautet, Surf. Sci. 356 (1996) L403.
[33] W. Dong, J. Hafner, Phys. Rev. B 56 (1997) 15396.
[34] R. Löber, D. Hennig, Phys. Rev. B 55 (1997) 4761.
[35] W. Dong, V. Ledentu, Ph. Sautet, A. Eichler, J. Hafner, Surf. Sci. 411 (1998) 123.
[36] V. Pallassana, M. Neurock, L.B. Hansen, B. Hammer, J.K. Nørskov, Phys. Rev. B 60 (1999) 6146.
[37] S. Wilke, D. Hennig, R. Löber, M. Methfessel, M. Scheffler, Surf. Sci. 307–309 (1994) 76.
[38] O.M. Løvvik, R.A. Olsen, Phys. Rev. B 58 (1998) 10890.
[39] G.W. Watson, R.P.K. Wells, D.J. Willock, G.J. Hutchings, J. Phys. Chem. B 105 (2001) 4889.
[40] N. Lopez, Z. Łodziana, F. Illas, M. Salmeron, Phys. Rev. Lett. 93 (2004) 146103.
[41] S. Hong, T.S. Rahman, Phys. Rev. B 75 (2007) 155405.
[42] K. Nobuhara, H. Nakanishi, H. Kasai, A. Okiji, J. Appl. Phys. 88 (2000) 6897.
[43] T. Mitsui, M.K. Rose, E. Fomin, D.F. Ogletree, M. Salmeron, Surf. Sci. 540 (2003) 5.
[44] C.T. Chan, S.G. Louie, Phys. Rev. B 27 (1983) 3325.
[45] M.P. Jigato, B. Coussens, D.A. King, J. Chem. Phys. 118 (2003) 5623.
[46] T. Mitsui, M.K. Rose, E. Fomin, D.F. Ogletree, M. Salmeron, Nature 422 (2003) 705.
[47] A. Groß, A. Dianat, Phys. Rev. Lett. 98 (2007) 206107.
[48] M. Johansson, J. Hoffmann Jørgensen, I. Chorkendorff, Rev. Sci. Instrum. 75 (2004) 2082.
[49] M. Johansson, T. Johannesen, J. Hoffman Jørgensen, I. Chorkendorff, Appl. Surf. Sci. 252 (2006) 3673.
[50] M. Johansson, O. Lytken, I. Chorkendorff, J. Chem. Phys. 128 (2008) 034706.
[51] M. Johansson, O. Lytken, I. Chorkendorff, Top. Catal. 46 (2007) 175.
[52] J.N. Russel Jr., S.M. Gates, J.T. Yates Jr., J. Chem. Phys. 85 (1986) 6792.
[53] B.L. Blackford, C.S. Arnold, P.J. Mulhern, M.H. Jericho, J. Appl. Phys. 76 (1994) 4054.
[54] J.A. Garcia, A. Mandelis, Rev. Sci. Instrum. 67 (1996) 3981.
[55] G.A. Frazier, R. Glosser, J. Less Common Metals 74 (1980) 89.
[56] R. Feenstra, G.J. de Bruin-Hordijk, H.L.M. Bakker, R. Griessen, D.G. de Groot, J. Phys. F 13 (1983) L13.
[57] M. Nicolas, L. Dumoulin, J.P. Burger, J. Appl. Phys. 60 (1986) 3125.
[58] A. Pundt, M. Suleiman, C. Bähtz, M.T. Reetz, R. Kirchheim, N.M. Jisrawi, Mater. Sci. Eng. B108 (2004) 19.
[59] H. Kobayashi, M. Yamauchi, H. Kitagawa, Y. Kubota, K. Kato, M. Takata, J. Am. Chem. Soc. 130 (2008) 1828.
[60] C. Sachs, A. Pundt, R. Kirchheim, M. Winter, M.T. Reetz, D. Fritsch, Phys. Rev. B 64 (2001) 075408.
[61] S.-Y. Huang, C.-D. Huang, B.-T. Chang, C.-T. Yeh, J. Phys. Chem. B 110 (2006) 21783.
[62] S. Kishore, J.A. Nelson, J.H. Adair, P.C. Eklund, J. Alloys Comp. 389 (2005) 234.
[63] M. Yamauchi, R. Ikeda, H. Kitagawa, M. Takata, J. Phys. Chem. C 112 (2008) 3294.
[64] C. Nützenadel, A. Züttel, D. Chartouni, G. Schmid, L. Schlapbach, Eur. Phys. J. D 8 (2000) 245.

[65] A. Züttel, Ch. Nützenadel, G. Schmid, Ch. Emmenegger, P. Sudan, L. Schlapbach, Appl. Surf. Sci. 162–163 (2000) 571.
[66] M. Suleiman, N.M. Jisrawi, O. Dankert, M.T. Reetz, C. Bähtz, R. Kirchheim, A. Pundt, J. Alloys Comp. 356–357 (2003) 644.
[67] M. Wilde, K. Fukutani, M. Naschitzki, H.-J. Freund, Phys. Rev. B 77 (2008) 113412.
[68] A. Stern, A. Resnik, D. Shaltiel, J. Phys. F: Met. Phys. 14 (1984) 1625.
[69] Dacapo Pseudopotential Code, Center for Atomic-scale Materials Design (CAMD), Technical University of Denmark, Lyngby, 2006, https://wiki.fysik.dtu.dk/dacapo%3e.
[70] M.C. Payne, M.P. Teter, D.C. Allan, T.A. Arias, J.D. Joannopoulos, Rev. Mod. Phys. 64 (1992) 1045.
[71] G. Kresse, J. Furtmüller, Comput. Mater. Sci. 6 (1996) 15.
[72] D. Vanderbilt, Phys. Rev. B 41 (1990) 7892.
[73] B. Hammer, L.B. Hansen, J.K. Nørskov, Phys. Rev. B 59 (1999) 7413.
[74] P.W. Atkins, Physical Chemistry, sixth ed., Oxford University Press, Oxford, 1998. p. 485, 925, 942.
[75] E. Skúlason, V. Tripkovic, M. Björketun, S. Gudmundsdóttir, G. Karlberg, J. Rossmeisl, T. Bligaard, H. Jónsson, J.K. Nørskov, in preparation.
[76] E. Skúlason, G.S. Karlberg, J. Rossmeisl, T. Bligaard, J. Greeley, H. Jónsson, J.K. Nørskov, Phys. Chem. Chem. Phys. 9 (2007) 3241.
[77] G. Henkelman, B. Uberuaga, H. Jónsson, J. Chem. Phys. 113 (2000) 9901.
[78] G. Henkelman, H. Jónsson, J. Chem. Phys. 113 (2000) 9978.
[79] J.P. Perdew, J.A. Chevary, S.H. Vosko, K.A. Jackson, M.R. Pederson, D.J. Singh, C. Fiolhais, Phys. Rev. B 46 (1992) 6671.